

# Starburst-Driven Galactic Outflows

## Unveiling the Suppressive Role of Cosmic Ray Halos

Leonard E. C. Romano<sup>1,2,3</sup>, Ellis R. Owen<sup>4,5</sup>, and Kentaro Nagamine<sup>4,6,7,8,9</sup>

<sup>1</sup> Universitäts-Sternwarte, Fakultät für Physik, Ludwig-Maximilians-Universität München, Scheinerstr. 1, D-81679 München, Germany e-mail: lromano@usm.lmu.de

<sup>2</sup> Max-Planck-Institut für extraterrestrische Physik, Giessenbachstr. 1, D-85741 Garching, Germany

<sup>3</sup> Excellence Cluster ORIGINS, Boltzmannstr. 2, D-85748 Garching, Germany

<sup>4</sup> Theoretical Astrophysics, Department of Earth and Space Science, Osaka University, 1-1 Machikaneyama, Toyonaka, Osaka 560-0043, Japan

<sup>5</sup> Astrophysical Big Bang Laboratory (ABBL), RIKEN Cluster for Pioneering Research, Wakō, Saitama 351-0198, Japan e-mail: ellis.owen@riken.jp

<sup>6</sup> Theoretical Joint Research, Forefront Research Center, Osaka University, 1-1 Machikaneyama, Toyonaka, Osaka 560-0043, Japan

<sup>7</sup> Kavli IPMU (WPI), UTIAS, The University of Tokyo, Kashiwa, Chiba 277-8583, Japan

<sup>8</sup> Department of Physics and Astronomy, University of Nevada, Las Vegas, 4505 S. Maryland Pkwy, Las Vegas, NV 89154-4002, USA

<sup>9</sup> Nevada Center for Astrophysics, University of Nevada, Las Vegas, 4505 S. Maryland Pkwy, Las Vegas, NV 89154-4002, USA

Received XXX; accepted YYY

### ABSTRACT

**Aims.** We investigate the role of cosmic ray (CR) halos in shaping the physical properties of starburst-driven galactic outflows.

**Methods.** We construct a model for galactic outflows driven by a continuous central injection of energy, gas and CRs, where the treatment of CRs accounts for the effect of CR pressure gradients on the flow dynamics. The model parameters are set by the effective properties of a starburst. By analyzing the asymptotic behavior of our model, we derive the launching criteria for starburst-driven galactic outflows and determine their corresponding outflow velocities.

**Results.** We find that, in the absence of CRs, stellar feedback can only launch galactic outflows if the star formation rate (SFR) surface density exceeds a critical threshold proportional to the dynamical equilibrium pressure. In contrast, CRs can always drive slow outflows. CR-driven outflows dominate in systems with SFR surface densities below the critical threshold, but their influence diminishes in highly star-forming systems. However, in older systems with established CR halos, the CR contribution to outflows weakens once the outflow reaches the galactic scale height, making CRs ineffective in sustaining outflows in such environments.

**Conclusions.** Over cosmic time, galaxies accumulate relic CRs in their halos, providing additional non-thermal pressure support that suppresses low-velocity CR-driven outflows. We predict that such low-velocity outflows are expected only in young systems that have yet to build significant CR halos. In contrast, fast outflows in starburst galaxies, where the SFR surface density exceeds the critical threshold, are primarily driven by thermal energy and remain largely unaffected by CR halos.

**Key words.** Galaxy winds – circumgalactic medium – cosmic rays – starburst galaxies

## 1. Introduction

Galaxies with high star-formation surface densities often host large-scale outflow winds. Such winds have been observed in local starbursts, such as Arp 220, M82, and NGC 253 (e.g., Bolatto et al. 2013; Leroy et al. 2015; Walter et al. 2017; Barcos-Muñoz et al. 2018) and are widespread at high-redshifts, where galaxies are typically more compact and have higher star-formation rates relative to their stellar mass (see, e.g. Sugahara et al. 2019; Nianias et al. 2024; Thompson & Heckman 2024). Outflow winds play an important role in redistributing energy, momentum, and baryons between the interstellar medium (ISM) and halos of galaxies. This makes them a key feedback component that regulates the evolution of galaxy ecosystems. Yet, despite their importance, a complete picture of the role they play remains unsettled (see Zhang 2018; Thompson & Heckman 2024, for reviews).

Detailed multi-wavelength observations of nearby starburst galaxies with outflows have revealed certain common features, including a bi-conical shape aligned along the minor axis of their

host galaxy (Veilleux et al. 2005), extensions reaching 10s of kpc into the halo (Veilleux et al. 2005; Zhang 2018), a terminal “cap” at a few kpc, e.g., at  $\sim 12$  kpc in M82 (see Lehnert et al. 1999; Tsuru et al. 2007), and the presence of entrained magnetic fields (e.g. Jones et al. 2019; Lopez-Rodriguez et al. 2021) and high-energy CR particles (for an overview, see Irwin et al. 2024).

Despite these apparent similarities, the physical configuration of individual galactic outflows can vary substantially. For instance, flow velocities ranging up to  $\sim 1,000$  km s<sup>-1</sup> have been reported (e.g. Bradshaw et al. 2013; Heckman et al. 2015; Ciccone et al. 2016; Cazzoli et al. 2016; Xu et al. 2022; Taylor et al. 2024), while densities and mass-loading factors span over 1.5 orders of magnitude (e.g. Xu et al. 2023a; Heckman et al. 2015). This diversity can be attributed to differences in the energy, matter, and momentum being supplied to an outflow by its host galaxy (Zhang 2018; Thompson & Heckman 2024), the underlying driving microphysics (Yu et al. 2020), and environ-

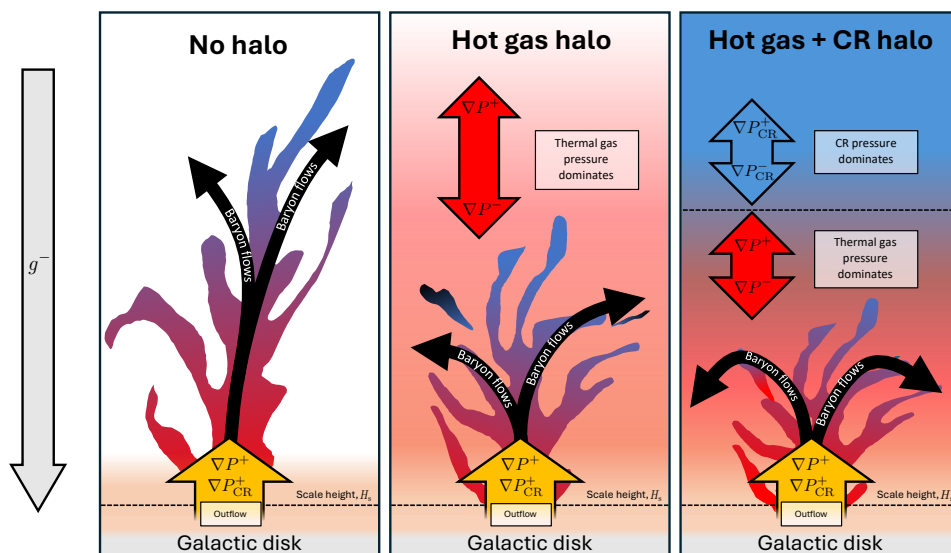


**Fig. 1.** Schematic of the structure of a starburst-driven outflow embedded in a galactic halo, propelled by thermal gas pressure and/or non-thermal CR pressure. The scale height of the warm ISM is indicated. All galaxies are embedded in a gravitational potential,  $g$ , which opposes the outflow. Superscripts  $+$  and  $-$  on quantities indicate whether each term contributes to or opposes the outflow, respectively. **Left:** In the absence of a substantial gas halo, outflowing gas is unconfined, allowing it to escape beyond the galaxy ecosystem against the galaxy’s gravitational potential. **Center:** As the galaxy builds up its stellar mass, feedback processes form a hot gas halo that suppresses the outflow, promoting baryonic recycling and enriching the CGM (see Ferrara et al. 2005; Shin et al. 2021). **Right:** When CRs are supplied to the halo, they accumulate over time, introducing a non-thermal halo component. Since non-thermal CR pressure gradients operate over larger length scales than thermal pressure gradients, an outflow erupting into the galaxy halo encounters distinct layers where thermally dominated and CR-dominated pressure gradients hinder its development.

mental factors — particularly the conditions of the surrounding halo.

Hot halo gas exerts inward pressure. This can oppose the development of a galactic outflow by reducing its velocity and limiting its extension compared to systems without a halo (e.g. Shin et al. 2021). By confining metal-enriched outflows and restricting the dispersal of ejecta, halo gas ram pressure has been considered to be instrumental in regulating baryonic recycling flows and enabling the enrichment of galaxies’ CGM (Ferrara et al. 2005). In addition to this thermal pressure from the hot gas, galaxy halos may also host a reservoir of CRs. These CRs may originate as a relic population that could be transported by advection, bubbles associated with outflows, or the activity of a central supermassive black hole (see e.g. Owen et al. 2019; Recchia et al. 2021; Shimoda & Inutsuka 2022).

Halo CRs can modify the structure of the circumgalactic medium (CGM) and alter baryonic flows within galaxy halos (for reviews, see Ruszkowski & Pfrommer 2023; Owen et al. 2023). Simulations of Milky-Way-mass galaxies suggest that CRs provide additional pressure support to sustain a multi-phase halo gas structure at low temperatures and can propel cool gas out to 100s of kpc (Butsky & Quinn 2018; Ji et al. 2020). CR-driven winds can even push gas beyond the virial radius (Quataert & Hopkins 2025). Due to the long CR survival time in halos, these feedback effects can continue to manifest long after the end of the mechanical processes that originally generated the CRs (Quataert & Hopkins 2025). Halo CRs can also operate alongside hot halo gas to provide an inward non-thermal pressure that counteracts developing outflows. This is illustrated in Fig. 1, which compares the suppressive effect of galaxy halos and the implications for baryonic recycling.

In this study, we assess the role of an extended CR halo in modifying the development of galactic winds driven by CR and

thermal gas pressure, and derive the criteria for the breakout of an outflow from a galaxy with a CR halo.

## 2. Starburst-driven Outflows in Galaxy Halos

The collective feedback from a central galactic starburst can initiate a blastwave, which may develop into a sustained galactic wind if the starburst activity is continuous. Typically, about one SN explodes per  $\sim 100 M_{\odot}$  of star formation, with the exact rate dependent on the choice of the stellar initial mass function (e.g. Leitherer et al. 1999). We can therefore link the supernova event rate  $\mathcal{R}_{\text{SN}} = \mathcal{R}_{-3} \text{ kyr}^{-1}$  to the SFR of a galaxy by  $\mathcal{R}_{\text{SF}} \sim 100 M_{\odot} \mathcal{R}_{\text{SN}}$ . Observationally, star formation activity is typically quantified using the SFR surface density,  $\Sigma_{\text{SFR}}$ . This can be related to  $\mathcal{R}_{\text{SF}}$  by considering that most star formation contributing to the blastwave occurs within a cylindrical region with a radius comparable to the disk scale height,  $\sim H_s$ , of a galaxy (defined by eq. A.2), i.e.  $\Sigma_{\text{SFR}} = \mathcal{R}_{\text{SF}} / (\pi H_s^2) = \Sigma_{\text{SFR},0} M_{\odot} \text{ yr}^{-1} \text{ kpc}^{-2}$ .

The injection rates of mass ( $\dot{M}_{\text{SB}} = M_{\text{ej}} \mathcal{R}_{\text{SN}}$ , for  $M_{\text{ej}} = M_{\text{ej},0} M_{\odot}$  as the typical supernova ejecta mass) and energy ( $\dot{E}_{\text{SB}} = E_{\text{SN}} \mathcal{R}_{\text{SN}}$ , for  $E_{\text{SN}} = 10^{51} E_{51} \text{ erg}$  as the typical mechanical energy supplied by a supernova) supplied to an expanding blastwave from a galactic starburst can be linked to the SFR through the mass- and energy-loading factors  $\eta_{\text{m}} \equiv \dot{M}_{\text{SB}} / \mathcal{R}_{\text{SF}} = 0.01 M_{\text{ej},0}$  and  $\eta_{\text{e}} \equiv \varepsilon_{\text{w}} \dot{E}_{\text{SB}} / (E_{\text{SN}} \mathcal{R}_{\text{SN}}) = \varepsilon_{\text{w}}$ , respectively, where  $\varepsilon_{\text{w}}$  is a thermalization efficiency factor accounting for energy dissipation in the system (see e.g. Thompson et al. 2016; Kim et al. 2017; Steinwandel et al. 2024). For convenience, we introduce the scaling parameters  $\eta_{\text{m},-2} = \eta_{\text{m}} / 0.01$ ,  $\eta_{\text{e},-2} = \eta_{\text{e}} / 0.01$  and  $\varepsilon_{\text{w},-2} = \varepsilon_{\text{w}} / 0.01$ . The supply of CRs to the wind is parametrized by  $f_{\text{CR}}$ , representing the CR energy fraction at the galactic mid-plane. In our model, these parameters are treated as constants, remaining fixed throughout the evolution of the outflow, and the

flow is considered to be driven by the combination of central thermal and kinetic energy-injection, and CR pressure gradients.

### 2.1. CR halos and their effects on outflows

Several observational studies have suggested the presence of extended CR reservoirs in galactic halos. These include a  $\gamma$ -ray halo around M31 reaching to 100s of kpc, which likely traces an interacting population of hadronic CRs (Recchia et al. 2021),  $\gamma$ -ray emission originating from halo clouds at kpc heights around the Milky Way (Tibaldo et al. 2015), and kpc-scale synchrotron emission from edge-on galaxies (e.g. Mulcahy et al. 2018; Mora-Partiarroyo et al. 2019). It has also been proposed that diffuse X-ray emission from the halos of Milky Way, M31, and lower-mass galaxies could originate from inverse Compton scattering, driven by a leptonic CR population (Hopkins et al. 2025).

The formation of CR halos is a consequence of CR production during galaxy evolution. The long energy loss times of hadronic CRs in these environments (see Appendix A.1) ensure that most of the CR energy density supplied to a galaxy halo during its development can survive to the present day. Galaxies with significant historical stellar mass buildup are expected to host rich CR halos, even if their current star formation activity is low. Observations in  $\gamma$ -rays tentatively support this distinction, with CR halos primarily identified around massive late-type galaxies, while lower-mass galaxies show no indications of hosting such structures (Pshirkov & Nizamov 2024).

To assess whether a CR halo can influence a developing outflow, the CR pressure contributions from both the halo and the outflow can be compared at a given altitude,  $z$  (see Appendix A; eqs. A.3 and A.7). For CRs to drive an outflow, the outward CR pressure must exceed the inward pressure from the halo CRs. When external and internal CR pressures become comparable, the driving effect of CR pressure gradients diminishes.

As illustrated in Fig. 1, the presence of a CR halo is expected to frustrate slow outflows if its scale height significantly exceeds the altitude where external and internal CR pressures are equal,  $z_{\text{CR}}$ . In units of the disk scale height,  $H_s$ , this CR pressure equilibrium height is given by:

$$z_{\text{CR}} \sim 1.5 \varepsilon_{w,-2}^{1/2} E_{51}^{1/2} \mathcal{R}_{-3}^{1/2} \sigma_1^{-2} v_{\infty,2}^{-1/2} H_s, \quad (1)$$

where  $\sigma = 10 \sigma_1$  km/s is the gas velocity dispersion, and  $v_{\infty,2}$  is the rescaled terminal flow velocity defined as  $v_{\infty} = 100 v_{\infty,2}$  km/s at large distances from the galactic plane. Equation 1 indicates that  $z_{\text{CR}}$  is typically located at low altitudes for most galaxies. This suggests that CR-driven outflows are easily suppressed by the presence of an extended CR halo, if the halo has a scale-height  $\gg H_s$ . Galactic winds in systems with a well-developed CR halo are therefore expected to experience suppression, with their driving primarily dependent on thermal and kinetic energy-injection rather than CR pressure.

### 2.2. Outflow breakout criterion and terminal velocity

For an outflow to break out from a galaxy, a minimum critical SFR surface density can be defined in the absence of a CR halo (see Appendix A.2). This is given by:

$$\Sigma_{\text{SFR},c} \gtrsim 2.14 n_0 \sigma_1^2 \eta_{e,-2}^{-1/2} \eta_{m,-2}^{-1/2} M_{\odot} \text{yr}^{-1} \text{kpc}^{-2}, \quad (2)$$

where  $n_{\text{H},\text{mp}} = n_0 \text{cm}^{-3}$  is introduced as the mid-plane gas number density. In a strong star-starburst (i.e. when  $\Sigma_{\text{SFR}} \gg \Sigma_{\text{SFR},c}$ ), the maximum flow speed that can develop tends towards an asymptotic limit (see eq. A.10).

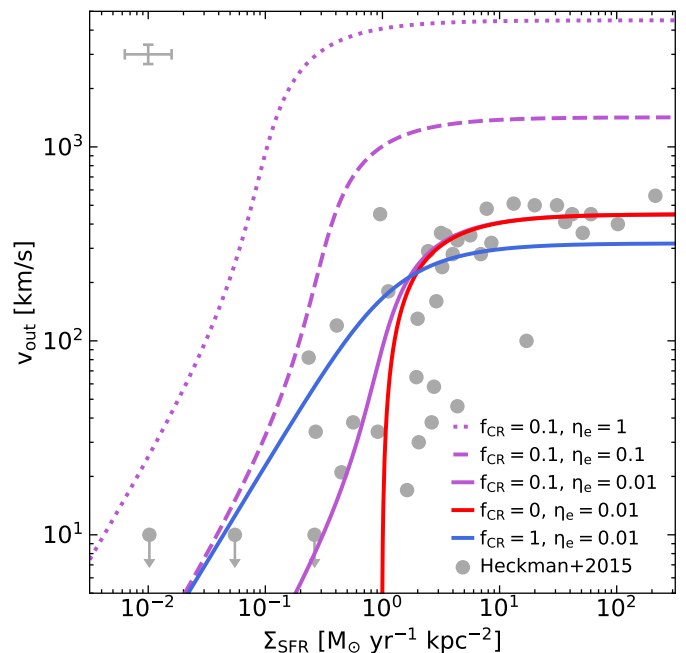


**Fig. 2.** Terminal outflow velocities as a function of star formation rate surface density for different choices of CR energy fractions,  $f_{\text{CR}}$ , and energy loading factors,  $\eta_e$ . The model predictions are compared with data from Heckman et al. (2015), which show measured outflow velocities for a sample of nearby starburst galaxies with stellar masses in the range  $\log_{10}(M_*/M_{\odot}) \in [7.1 - 10.9]$ . Typical uncertainties are indicated in the top-left corner. The model with  $\eta_e \sim 0.01$  and  $f_{\text{CR}} \sim 0.1$  provides a good match with the observed data. Models with higher energy loading values ( $\eta_e$ ) generally predict outflow velocities in excess of the observations. The transition from slow outflows in weak starbursts to fast outflows in strong starbursts is best captured by models with  $f_{\text{CR}} > 0$ .

CR-driven outflows can always be launched without a specific breakout criterion. However, in weak star formation scenarios (i.e.  $\Sigma_{\text{SFR}} \ll \Sigma_{\text{SFR},c}$ ), only very slow flow velocities can be achieved:

$$v_{\infty}^{\text{weak}} \rightarrow 237 f_{\text{CR}} \eta_{e,-2} \Sigma_{\text{SFR},0} \sigma_1^{-2} n_0^{-1} \text{ km s}^{-1}. \quad (3)$$

In this regime, the CR pressure equilibrium height reduces to:

$$z_{\text{CR}}^{\text{weak}} \rightarrow 1.85 f_{\text{CR}}^{-1/2} H_s \quad (4)$$

which decreases as the CR supply to the system increases. This indicates that a CR halo strongly suppresses weak outflows that rely on CR driving (c.f. the right panel of Fig. 1).

In the strong starburst limit (when  $\Sigma_{\text{SFR}} \gg \Sigma_{\text{SFR},c}$ ), much faster terminal velocities are expected:

$$v_{\infty}^{\text{strong}} \rightarrow 10^3 \eta_{e,-2}^{1/2} \eta_{m,-2}^{-1/2} \frac{\sqrt{1+f_{\text{CR}}} + \sqrt{1-f_{\text{CR}}}}{2} \text{ km s}^{-1}. \quad (5)$$

The CR pressure equilibrium height in this regime is then

$$z_{\text{CR}}^{\text{strong}} \rightarrow 0.47 \varepsilon_{w,-2}^{1/4} E_{51}^{1/4} M_{\text{ej},0}^{1/4} \mathcal{R}_{-3}^{1/2} \sigma_1^{-2} H_s. \quad (6)$$

Although the inward halo CR pressure overtakes the outward flow-driving CR pressure near the disk scale height, the independence of  $z_{\text{CR}}^{\text{strong}}$  from  $f_{\text{CR}}$  suggests that outflows in this regime are momentum-dominated. Such outflows are unlikely to be significantly influenced by the presence of a CR halo, with thermal gas pressure likely playing a more critical role in regulating flow dynamics (see the central panel of Fig. 1).

The terminal velocities predicted by our model allow for comparison with observations. Figure 2 shows terminal outflow velocities as a function of SFR surface density for a fiducial model with (dimensionless) parameters  $n_0 = 1$ ,  $\sigma_1 = 1$ ,  $\eta_{m,-2} = 5$ , and varying values of  $f_{\text{CR}}$  and  $\eta_{e,-2}$  as indicated in the legend. These calculations assume that all galaxies in the sample share a similar dynamical equilibrium pressure,  $P_{\text{DE}} \sim \rho_{\text{mp}} \sigma^2 \sim G\Sigma^2$  (Ostriker & Kim 2022) for  $\rho_{\text{mp}}$  as the galactic mid-plane gas volume density and  $\Sigma$  as the corresponding surface density that sets  $\Sigma_{\text{SFR},c}$ . For comparison, observed outflow velocities for a sample of nearby starburst galaxies with stellar masses in the range  $\log_{10}(M_*/M_\odot) \in [7.1 - 10.9]$  are also shown (Heckman et al. 2015). Our model captures the general trend of observed flow velocities with parameter choices of  $\varepsilon_{w,-2} \sim \eta_{e,-2} \sim 1$  and  $\eta_{m,-2} \sim M_{\text{ej},0} \sim 5$ . These choices align well with the energy and mass loading factors reported in numerical simulations of galactic outflows at altitudes of a few kpc (e.g. Kim & Ostriker 2018; Rathjen et al. 2021; Steinwandel et al. 2024; Kjellgren et al. 2025).

### 3. Discussion and Implications

The structure of galactic winds has been extensively studied through theoretical approaches (e.g. Chevalier & Clegg 1985; Fielding & Bryan 2022; Modak et al. 2023), detailed numerical simulations (e.g. Kim & Ostriker 2018; Vasiliev et al. 2023; Kjellgren et al. 2025) and observational studies (e.g. Krieger et al. 2019; Xu et al. 2023b; Bolatto et al. 2024). These studies have shown that galactic winds are ubiquitous, particularly among star-forming galaxies, and that galaxies with high SFRs tend to drive faster and hotter winds. However, not all galaxies show clear signatures of outflows. Some systems show that gas launched from the ISM is recycled within a galaxy ecosystem rather than expelled (Marasco et al. 2023). While the qualitative framework for wind launching is well established (see Thompson & Heckman 2024, for a review), few studies quantify outflow launching conditions (e.g. Heckman et al. 2015; Orr et al. 2022).

Heckman et al. (2015) examined outflow speeds of galactic winds in a sample of nearby starbursts, and reported a sharp drop in flow velocities when the central SFR surface density fell below a critical threshold of  $\Sigma_{\text{SFR},c} \sim 1 M_\odot \text{yr}^{-1} \text{kpc}^{-2}$ . Our model shows that this critical SFR surface density arises due to the depth of the gravitational potential, which can only be overcome by sufficiently strong starbursts. The predicted value aligns with observations when considering typical dynamical equilibrium pressures set by the weight of the ISM, together with wind-loading parameters that are consistent with recent numerical studies of galactic winds in dwarf (Steinwandel et al. 2024) and spiral galaxies in the local Universe (Kjellgren et al. 2025). However, we note that other studies find significantly higher mass and energy loading, depending on the methodology used (e.g. Muratov et al. 2015; Smith et al. 2024).

Orr et al. (2022) investigated the feedback from star formation in a marginally Toomre-stable disk. They proposed that a young star cluster could launch an outflow if the starburst-driven shock reaches the disk scale height before its speed drops below the ISM's velocity dispersion. By assuming the formation of one star cluster per orbital timescale, they derived an expression for the critical SFR surface density, which is in rough agreement with the threshold found observationally by Heckman et al. (2015). However, their study does not account for the effects of gravity, which would alter the wind-launching criterion.

Most numerical simulations of starburst-driven galactic winds show that the inclusion of CRs improves their ability to drive warm outflows with high mass-loading factors (e.g. Girichidis et al. 2016; Rathjen et al. 2021; Chan et al. 2022; Armillotta et al. 2024). This is in agreement with our results, which indicate that outflow speed in the CR-dominated regime is independent of the mass-loading factor, and suggest that CR-driven winds can sustain substantial mass-loading before being significantly slowed. However, current numerical models do not typically include a pre-existing CR halo in their initial conditions. Instead, they only model the accumulation of CRs within a galaxy ecosystem over time, usually as a consequence of stellar feedback. The widespread findings of substantial feedback impacts from CR-driven outflows in the literature may reflect this limitation — a situation that would have certain parallels with earlier numerical studies that lacked CGM thermal pressure, leading to unrealistically strong outflows in simulations of isolated galaxies (Shin et al. 2021).

At high redshift, several studies have reported high outflow velocities up to  $1,000 \text{ km s}^{-1}$  (Sugahara et al. 2019; Xu et al. 2022). In general, higher outflow speeds require higher energy loading factors and lower mass loading factors. Observations suggest that high-redshift galaxies tend to be compact and turbulent (Genzel et al. 2023), with high gas fractions and surface densities (e.g. Genzel et al. 2011), as well as low metallicities (Maiolino et al. 2008). Since the critical SFR surface density scales with the dynamical equilibrium pressure as  $\Sigma_{\text{SFR},c} \propto P_{\text{DE}} \propto \Sigma^2$ , thermally-driven outflows become ineffective in a highly turbulent, high surface-density environment. On the other hand, lower metallicities result in longer cooling times, leading to higher momentum-loading (Oku et al. 2022). If mass-loading factors in high-redshift galaxies are comparable to those in low-redshift galaxies, then lower metallicities could explain the high observed outflow velocities in high-redshift galaxies, provided that the increased ISM weight does not suppress outflows.

Curiously, the critical SFR surface density exhibits a stronger dependence on gas surface density than on the SFR surface density itself, which follows  $\Sigma_{\text{SFR},c} \propto \Sigma^{1.4}$  (Kennicutt 1989). This suggests that, counterintuitively, fast thermally-powered galactic outflows are expected to be more common at low surface densities, such as in dwarf galaxies, while being suppressed in extreme star-forming environments - including massive clumps in high-redshift galaxies (Genzel et al. 2011) and the proposed feedback-free starburst galaxies at  $z \sim 10$  (Finkelstein et al. 2023; Dekel et al. 2023). At high redshifts, CR-driven slow outflows may be more prevalent in these systems, as there would not have been sufficient time for them to establish a CR halo capable of suppressing outflows. Indeed, highly mass-loaded outflows are essential for regulating star formation and explaining observed metallicity trends at high redshift (Toyouchi et al. 2025), which could naturally be accounted for by CR-driven outflows.

### 4. Conclusions

In this study, we constructed a galactic outflow model driven by a continuous central feedback source, including the effects of CR pressure in the outflow and surrounding galaxy halo. We applied this model to a starburst galaxy to assess how the presence of a CR halo may influence outflow development. We found:

1. In the absence of CRs, galactic outflows are only launched if the SFR surface density exceeds a critical threshold proportional to the dynamic equilibrium pressure. At high SFR sur-

face densities, these momentum-driven outflows approach the ejecta speed, reaching up to 1,000s of  $\text{km s}^{-1}$ .

2. CRs can always drive slow outflows. We identified two different regimes: slow, CR-dominated outflows at SFR surface densities below the critical threshold, and fast, momentum-driven outflows at high SFR surface densities.
3. In the presence of an extended CR halo, CRs become ineffective in sustaining outflows beyond the galactic scale height, leading to the suppression of CR-driven winds.

While our simplified approach is subject to substantial limitations (see Appendix B), it provides useful insights into the qualitative behavior of starburst-driven outflows and the influence of a CR halo. However, more detailed studies - including numerical simulations with CR halos as an initial condition - are needed to properly explore the physical impacts of CRs on the dynamical processes within galaxy halos.

*Acknowledgements.* This research was funded in part by the Deutsche Forschungsgemeinschaft (DFG, German Research Foundation) under Germany's Excellence Strategy – EXC 2094 – 390783311. E.R.O. is an international research fellow under the Postdoctoral Fellowship of the Japan Society for the Promotion of Science (JSPS), supported by JSPS KAKENHI Grant Number JP22F22327, and also acknowledges support from the RIKEN Special Postdoctoral Researcher Program for junior scientists. This work was supported in part by the MEXT/JSPS KAKENHI grant numbers 20H00180, 22K21349, 24H00002, and 24H00241 (K.N.). K.N. acknowledges the support from the Kavli IPMU, the World Premier Research Centre Initiative (WPI), UTIAS, the University of Tokyo.

## References

- Armillotta, L., Ostriker, E. C., Kim, C.-G., & Jiang, Y.-F. 2024, *ApJ*, 964, 99
- Barcos-Muñoz, L., Aalto, S., Thompson, T. A., et al. 2018, *ApJ*, 853, L28
- Behrendt, M., Burkert, A., & Schartmann, M. 2015, *MNRAS*, 448, 1007
- Bolatto, A. D., Levy, R. C., Tarantino, E., et al. 2024, *ApJ*, 967, 63
- Bolatto, A. D., Warren, S. R., Leroy, A. K., et al. 2013, *Nature*, 499, 450
- Bradshaw, E. J., Almaini, O., Hartley, W. G., et al. 2013, *MNRAS*, 433, 194
- Butsky, I. S. & Quinn, T. R. 2018, *ApJ*, 868, 108
- Cazzoli, S., Arribas, S., Maiolino, R., & Colina, L. 2016, *A&A*, 590, A125
- Chan, T. K., Kereš, D., Gurvich, A. B., et al. 2022, *MNRAS*, 517, 597
- Chan, T. K., Kereš, D., Hopkins, P. F., et al. 2019, *MNRAS*, 488, 3716
- Chevalier, R. A. & Clegg, A. W. 1985, *Nature*, 317, 44
- Cicone, C., Maiolino, R., & Marconi, A. 2016, *A&A*, 588, A41
- Dekel, A., Sarkar, K. C., Birnboim, Y., Mandelker, N., & Li, Z. 2023, *MNRAS*, 523, 3201
- Devine, D. & Bally, J. 1999, *ApJ*, 510, 197
- Ferrara, A., Scannapieco, E., & Bergeron, J. 2005, *ApJ*, 634, L37
- Fielding, D. B. & Bryan, G. L. 2022, *ApJ*, 924, 82
- Finkelstein, S. L., Bagley, M. B., Ferguson, H. C., et al. 2023, *ApJ*, 946, L13
- Genzel, R., Jolly, J. B., Liu, D., et al. 2023, *ApJ*, 957, 48
- Genzel, R., Newman, S., Jones, T., et al. 2011, *ApJ*, 733, 101
- Girichidis, P., Naab, T., Walch, S., et al. 2016, *ApJ*, 816, L19
- Heckman, T. M., Alexandroff, R. M., Borthakur, S., Overzier, R., & Leitherer, C. 2015, *ApJ*, 809, 147
- Herenz, E. C., Kusakabe, H., & Maulick, S. 2025, *arXiv e-prints*, [arXiv:2502.16969](https://arxiv.org/abs/2502.16969)
- Hopkins, P. F., Butsky, I. S., Ji, S., & Kereš, D. 2023, *MNRAS*, 522, 2936
- Hopkins, P. F., Butsky, I. S., Panopoulou, G. V., et al. 2022, *MNRAS*, 516, 3470
- Hopkins, P. F., Quataert, E., Ponnada, S. B., & Silich, E. 2025, *arXiv e-prints*, [arXiv:2501.18696](https://arxiv.org/abs/2501.18696)
- Irwin, J., Beck, R., Cook, T., et al. 2024, *Galaxies*, 12, 22
- Ji, S., Chan, T. K., Hummels, C. B., et al. 2020, *MNRAS*, 496, 4221
- Jones, T. J., Dowell, C. D., Lopez Rodriguez, E., et al. 2019, *ApJ*, 870, L9
- Karwin, C. M., Murgia, S., Campbell, S., & Moskalenko, I. V. 2019, *ApJ*, 880, 95
- Kennicutt, Jr., R. C. 1989, *ApJ*, 344, 685
- Kim, C.-G. & Ostriker, E. C. 2015, *ApJ*, 802, 99
- Kim, C.-G. & Ostriker, E. C. 2018, *ApJ*, 853, 173
- Kim, C.-G., Ostriker, E. C., & Raileanu, R. 2017, *ApJ*, 834, 25
- Kjellgren, K., Girichidis, P., Göller, J., et al. 2025, *arXiv e-prints*, [arXiv:2502.02635](https://arxiv.org/abs/2502.02635)
- Koo, B.-C. & McKee, C. F. 1990, *ApJ*, 354, 513
- Krieger, N., Bolatto, A. D., Walter, F., et al. 2019, *ApJ*, 881, 43
- Lancaster, L., Ostriker, E. C., Kim, C.-G., Kim, J.-G., & Bryan, G. L. 2024, *ApJ*, 970, 18
- Laumbach, D. D. & Probst, R. F. 1969, *Journal of Fluid Mechanics*, 35, 53
- Lehnert, M. D., Heckman, T. M., & Weaver, K. A. 1999, *ApJ*, 523, 575
- Leitherer, C., Schaerer, D., Goldader, J. D., et al. 1999, *ApJS*, 123, 3
- Leroy, A. K., Walter, F., Martini, P., et al. 2015, *ApJ*, 814, 83
- Lopez-Rodriguez, E., Guerra, J. A., Asgari-Targhi, M., & Schmelz, J. T. 2021, *ApJ*, 914, 24
- Maiolino, R., Nagao, T., Grazian, A., et al. 2008, *A&A*, 488, 463
- Marasco, A., Belfiore, F., Cresci, G., et al. 2023, *A&A*, 670, A92
- Modak, S., Quataert, E., Jiang, Y.-F., & Thompson, T. A. 2023, *MNRAS*, 524, 6374
- Mora-Partiarroyo, S. C., Krause, M., Basu, A., et al. 2019, *A&A*, 632, A10
- Mulcahy, D. D., Horneffer, A., Beck, R., et al. 2018, *A&A*, 615, A98
- Muratov, A. L., Kereš, D., Faucher-Giguère, C.-A., et al. 2015, *MNRAS*, 454, 2691
- Nianias, J., Lim, J., & Yeung, M. 2024, *ApJ*, 963, 19
- Oku, Y., Tomida, K., Nagamine, K., Shimizu, I., & Cen, R. 2022, *ApJS*, 262, 9
- Orr, M. E., Fielding, D. B., Hayward, C. C., & Burkhardt, B. 2022, *ApJ*, 932, 88
- Ostriker, E. C. & Kim, C.-G. 2022, *ApJ*, 936, 137
- Ostriker, J. P. & McKee, C. F. 1988, *Reviews of Modern Physics*, 60, 1
- Owen, E. R., Jacobsen, I. B., Wu, K., & Surajbali, P. 2018, *MNRAS*, 481, 666
- Owen, E. R., Jin, X., Wu, K., & Chan, S. 2019, *MNRAS*, 484, 1645
- Owen, E. R., Wu, K., Inoue, Y., Yang, H. Y. K., & Mitchell, A. M. W. 2023, *Galaxies*, 11, 86
- Pshirkov, M. S. & Nizamov, B. A. 2024, *arXiv e-prints*, [arXiv:2410.02066](https://arxiv.org/abs/2410.02066)
- Quataert, E. & Hopkins, P. F. 2025, *arXiv e-prints*, [arXiv:2502.01753](https://arxiv.org/abs/2502.01753)
- Rathjen, T.-E., Naab, T., Girichidis, P., et al. 2021, *MNRAS*, 504, 1039
- Recchia, S., Gabici, S., Aharonian, F. A., & Niro, V. 2021, *ApJ*, 914, 135
- Ruszkowski, M. & Pfrommer, C. 2023, *A&A Rev.*, 31, 4
- Shimoda, J. & Inutsuka, S.-i. 2022, *ApJ*, 926, 8
- Shin, E.-J., Kim, J.-H., & Oh, B. K. 2021, *ApJ*, 917, 12
- Smith, M. C., Fielding, D. B., Bryan, G. L., et al. 2024, *MNRAS*, 527, 1216
- Steinwandel, U. P., Kim, C.-G., Bryan, G. L., et al. 2024, *ApJ*, 960, 100
- Su, M., Slatyer, T. R., & Finkbeiner, D. P. 2010, *ApJ*, 724, 1044
- Sugahara, Y., Ouchi, M., Harikane, Y., et al. 2019, *ApJ*, 886, 29
- Taylor, E., Maltby, D., Almaini, O., et al. 2024, *MNRAS*, 535, 1684
- Thompson, T. A. & Heckman, T. M. 2024, *ARA&A*, 62, 529
- Thompson, T. A., Quataert, E., Zhang, D., & Weinberg, D. H. 2016, *MNRAS*, 455, 1830
- Tibaldo, L., Digel, S. W., Casandjian, J. M., et al. 2015, *ApJ*, 807, 161
- Toyouchi, D., Yajima, H., Ferrara, A., & Nagamine, K. 2025, *arXiv e-prints*, [arXiv:2502.12538](https://arxiv.org/abs/2502.12538)
- Tsuru, T. G., Ozawa, M., Hyodo, Y., et al. 2007, *PASJ*, 59, 269
- Vasiliev, E. O., Drozdov, S. A., Nath, B. B., Dettmar, R.-J., & Shchekinov, Y. A. 2023, *MNRAS*, 520, 2655
- Veilleux, S., Cecil, G., & Bland-Hawthorn, J. 2005, *ARA&A*, 43, 769
- Walter, F., Bolatto, A. D., Leroy, A. K., et al. 2017, *ApJ*, 835, 265
- Xu, X., Heckman, T., Henry, A., et al. 2022, *ApJ*, 933, 222
- Xu, X., Heckman, T., Henry, A., et al. 2023a, *ApJ*, 948, 28
- Xu, X., Heckman, T., Yoshida, M., Henry, A., & Ohyama, Y. 2023b, *ApJ*, 956, 142
- Yang, H. Y. K., Gaspari, M., & Marlow, C. 2019, *ApJ*, 871, 6
- Yu, B. P. B., Owen, E. R., Wu, K., & Ferreras, I. 2020, *MNRAS*, 492, 3179
- Zhang, D. 2018, *Galaxies*, 6, 114
- Zubovas, K. & Nayakshin, S. 2012, *MNRAS*, 424, 666

## Appendix A: Halo and Outflow model

### Appendix A.1: Halo model and CR timescales

In our model, the galaxy halo consists of a thermal gas component and a non-thermal CR component. The gas is treated as an infinite slab in vertical hydrostatic equilibrium, with a density profile given by:

$$\rho(z) = \rho_{\text{mp}} \cosh^{-2}\left(\frac{z}{H_s}\right), \quad (\text{A.1})$$

and velocity dispersion  $\sigma = 10 \sigma_1 \text{ km s}^{-1}$ , where  $\rho_{\text{mp}} = \mu m_{\text{H}} n_{\text{H, mp}}$  is the mid-plane gas density,  $\mu = 1.4$  is the mean atomic weight,  $n_{\text{H, mp}} = n_0 \text{ cm}^{-3}$  is the number density of the gas, and where the scale height of the is given by:

$$H_s = \frac{\sigma}{\sqrt{2\pi G \rho_{\text{mp}}}} \sim 338 \sigma_1 n_0^{-0.5} \text{ pc} \quad (\text{A.2})$$

(Behrendt et al. 2015). The expected profile of the CR component in the halo is uncertain and depends on the underlying CR transport physics, which remain unsettled. It has been suggested that buoyant bubbles may redistribute CRs in the halo (Recchia et al. 2021). Such bubbles, blown by SN-powered winds in starburst regions of a galaxy (e.g. Herenz et al. 2025), may be associated with outflows when they begin to fragment (e.g., above a cap similar to that seen in M82; Devine & Bally 1999), or could even be attributed to buoyant structures inflated by intensive energetic outbursts akin to the Galactic *Fermi* bubbles (e.g. Su et al. 2010; Zubovas & Nayakshin 2012; Recchia et al. 2021) analogous to AGN-inflated bubbles in Galaxy clusters (e.g. Yang et al. 2019). Observations of M31 do not yet strongly favor a particular CR distribution profile (Karwin et al. 2019), and detailed physical modeling of the CR halo is beyond the scope of the current work. We therefore adopt a simple spatially uniform CR distribution in the halo, effectively treating it as a CR bath in which an outflow develops. This approach is sufficient to obtain qualitative insights into the effects of a CR halo on outflow development, with more detailed modeling of CR transport mechanisms in galaxy halos left to future work.

To achieve a sensible normalization at low altitudes where CR pressure most strongly influences outflow development, the CR content of the halo is set to match the CR energy fraction at the galactic mid-plane. The halo CR pressure can then be expressed as:

$$P_{\text{CR, ext}} = \frac{\gamma_{\text{CR}} - 1}{\gamma - 1} f_{\text{CR}} \rho_{\text{mp}} \sigma^2, \quad (\text{A.3})$$

where the thermal gas adiabatic index is  $\gamma = 5/3$ , and the CR fluid adiabatic index is  $\gamma_{\text{CR}} = 4/3$ . This configuration creates a layered halo structure, with thermal gas pressure dominating at low altitudes and CR pressure becoming more important at higher altitudes (see the right panel of Fig. 1).

The CRs in the galaxy halo are likely primarily hadronic. This is because fast electron cooling in typical galactic conditions limits the electron population. Once deposited in the halo, CR hadrons experience few interaction or energy loss channels, allowing them to survive over Gyr timescales (see Fig. A.1). Adiabatic losses, streaming losses, and diffusive energy gains in micro-turbulence have only modest effects on the overall CR spectrum. Detailed simulations show that these processes rarely impact CR energies significantly in galaxy halos, typically contributing no more than 10 percent level corrections (Chan et al. 2019; Hopkins et al. 2022). We therefore neglect these effects

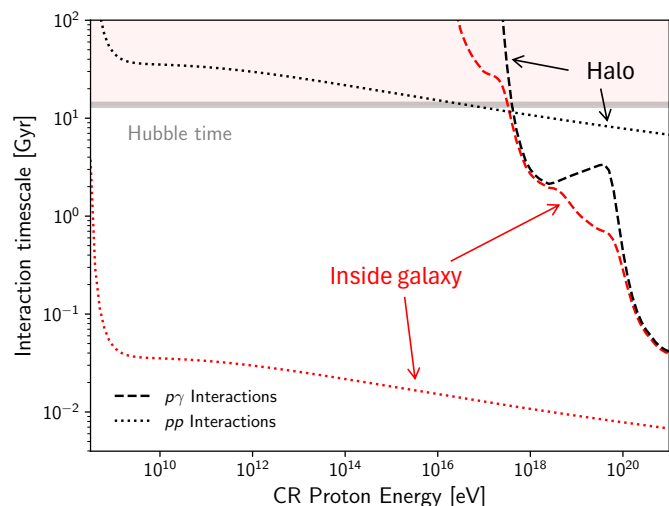


**Fig. A.1.** Characteristic timescales for a CR proton to undergo a hadronic interaction with ambient gas (pp interactions) or radiation (p $\gamma$  interactions) shown for typical conditions in the galaxy interior (red lines) and halo (black lines). For the galaxy interior, we adopt a gas density of  $1 \text{ cm}^{-3}$  and stellar radiation fields consisting of a stellar component with  $T = 7100 \text{ K}$  and an energy density of  $\sim 0.7 \text{ eV cm}^{-3}$ , with a dust component at  $T = 60 \text{ K}$  and an energy density of  $\sim 0.3 \text{ eV cm}^{-3}$ . For halo conditions, we consider a reduced gas density of  $10^{-3} \text{ cm}^{-3}$ , with radiation energy densities scaled down by a factor of 100. p $\gamma$  losses with cosmological microwave background radiation at  $z = 0$  are included for both galaxy interior and halo conditions, with photo-pair and photo-pion interactions occurring at the same rate in both environments. The Hubble timescale is shown in gray. Interaction timescales exceeding this (i.e. within the shaded pink region) practically do not occur. For an overview of these hadronic CR interaction processes and timescale calculations, see Owen et al. (2018).

in our model. Without significant cooling or absorption channels, CR hadrons are expected to accumulate in the galaxy halo, forming a fossil record of the host galaxy's CR power generation history.

### Appendix A.2: Outflow model

We consider that an outflow is driven by a continuous injection of energy, momentum, CRs, and thermal gas, forming an expanding super-bubble that launches a galactic wind. This approach allows us to establish a criterion for wind launching and derive an analytical expression for the outflow velocity. To do this, we start from the blastwave equation of motion (Ostriker & McKee 1988) under the thin-shell and sector approximations (e.g. Laubach & Probst 1969; Koo & McKee 1990), to derive an analytically tractable equation of motion suitable for modeling CR-driven outflows:

$$M \ddot{z} = (\Delta P + \Delta P_{\text{CR}} - \rho \dot{z}^2) \dot{z}^2 + M g + \frac{\dot{M}_{\text{SB}}}{4\pi} (v_{\text{ej}} - \dot{z}) \quad (\text{A.4})$$

Here  $z = z(t)$  is the shock radius at time  $t$  after the onset of shock expansion,  $\dot{z}$  and  $\ddot{z}$  are the instantaneous expansion velocity and acceleration of a thin shell following the expanding shock,  $M = \int \rho z^2 dz$  is the swept-up mass, and  $\Delta P$  and  $\Delta P_{\text{CR}}$  are the thermal and non-thermal pressure differences between the shocked and the un-shocked gas, respectively. The gravitational acceleration,  $g$ , for a single-component, isothermal slab in vertical hydrostatic

equilibrium is given by:

$$g = -2 \frac{\sigma^2}{H_s} \tanh\left(\frac{z}{H_s}\right). \quad (\text{A.5})$$

The speed of the ejecta,  $v_{\text{ej}}$ , is:

$$v_{\text{ej}} = \sqrt{2\varepsilon_w (1 - f_{\text{CR}}) E_{\text{SN}}/M_{\text{ej}}}. \quad (\text{A.6})$$

Other terms retain the definitions provided in the main text (see section 2).

We set  $\Delta P = 0$  to account for the fact that the SBs generally become radiative, and quickly enter a rapidly-cooling wind phase (e.g. Kim & Ostriker 2015; Oku et al. 2022). While the expansion of such rapidly cooling winds is still formally energy-driven, the coupling between the hot interior and the shell leads to dynamics that are equivalent to those of a momentum-driven wind, but with a slightly boosted momentum injection rate in comparison to that at the source (Lancaster et al. 2024). We account for this boost by means of the energy efficiency factor  $\varepsilon_w$ .

We model the CRs as a non-thermal fluid with an adiabatic index of  $\gamma_{\text{CR}} = 4/3$ , assuming a uniform pressure distribution immediately behind the shock. The CR pressure then evolves as:

$$P_{\text{CR, in}} = 3(\gamma_{\text{CR}} - 1) \frac{f_{\text{CR}} \varepsilon_w (\dot{E}_{\text{SB}}/4\pi) t}{z^3}. \quad (\text{A.7})$$

As the outflow reaches a steady state (i.e., over a timescale when the flow reaches its asymptotic limit at high altitudes), the mass it has swept up is given by:

$$\begin{aligned} M_{\infty} &= \int_0^{\infty} \rho(z) z^2 dz \\ &= \frac{\pi^2}{12} \rho_{\text{mp}} H_s^3 \sim 10^6 \sigma_1^3 n_0^{-1/2} M_{\odot}. \end{aligned} \quad (\text{A.8})$$

To analyze the properties of the outflow, we consider steady-state solutions with  $\dot{z} \rightarrow v_{\infty} = 100 v_{\infty,2} \text{ km s}^{-1}$  in the limit where  $z = v_{\infty} t \gg H_s$ , and where the mass of the shell is dominated by the swept-up mass, i.e.,  $(\dot{M}_{\text{SB}}/4\pi) t \ll M_{\infty}$ . In this limit, we can rewrite eq. A.4 as:

$$0 = \Delta P_{\text{CR}} z^2 - 2M_{\infty} \frac{\sigma^2}{H_s} + \frac{\dot{M}_{\text{SB}}}{4\pi} (v_{\text{ej}} - v_{\infty}). \quad (\text{A.9})$$

When external CR pressure is absent ( $\Delta P_{\text{CR}} = P_{\text{CR, in}}$ ), this reduces to a quadratic form with a single positive solution:

$$v_{\infty} = \frac{v_{\text{ej}}}{2\sqrt{1 - f_{\text{CR}}}} \left( \delta + \sqrt{\delta^2 + 2f_{\text{CR}}} \right), \quad (\text{A.10})$$

where

$$\delta = \sqrt{1 - f_{\text{CR}}} - \frac{\mathcal{R}_c}{\mathcal{R}_{\text{SN}}} \quad (\text{A.11})$$

and

$$\mathcal{R}_c^{-1} \sim 0.13 \varepsilon_{w,-2}^{1/2} E_{51}^{1/2} M_{\text{ej},0}^{1/2} \sigma_1^{-4} \text{ kyr}. \quad (\text{A.12})$$

In the absence of CRs, there are no outflow solutions when  $\mathcal{R}_{\text{SN}} \leq \mathcal{R}_c$ . On the other hand, when CRs are present, outflow solutions are always possible. For weak sources with  $\mathcal{R}_{\text{SN}} \ll \mathcal{R}_c$ , the outflow reaches very slow asymptotic speeds:

$$v_{\infty}^{\text{weak}} \rightarrow 66 f_{\text{CR}} \varepsilon_{w,-2} E_{51} \mathcal{R}_{-3} \sigma_1^{-4} \text{ km s}^{-1}. \quad (\text{A.13})$$

However, in the strong source limit where  $\mathcal{R}_{\text{SN}} \gg \mathcal{R}_c$ , the outflow velocities are much higher, approaching:

$$v_{\infty}^{\text{strong}} \rightarrow 10^3 \varepsilon_{w,-2}^{1/2} E_{51}^{1/2} M_{\text{ej},0}^{-1/2} \frac{\sqrt{1 + f_{\text{CR}}} + \sqrt{1 - f_{\text{CR}}}}{2} \text{ km s}^{-1}. \quad (\text{A.14})$$

## Appendix B: Model Limitations and Assumptions

Our model invokes a number of approximations and assumptions. While we consider our results to be qualitatively robust, future developments that relax these assumptions may provide more refined insights. Here, we assess the validity of our assumptions and approximations and discuss their potential impact on our results.

**Density Profile and Gravitational Field.** The density profile in eq. (A.1) represents an isothermal, single-component atmosphere in vertical hydrostatic equilibrium, providing a reasonably accurate description near the mid-plane. However, the presence of molecular gas and a young stellar disk could create a deeper potential well, leading to a more compact density profile that may affect the early stages of shock breakout. Moreover, explicitly modeling the gravitational potential of different galaxy components (e.g. the bulge, disk and dark-matter halo) could modify flow properties (see Shimoda & Inutsuka 2022), and this can be affected by the detailed gas distribution throughout the galaxy and inner halo. However, the outflow properties at high altitudes (above  $\sim 100$  kpc) are unlikely to be significantly impacted if the overall gas surface density and wind loading remain unchanged.

**Halo Gas Properties.** In the halo, the multi-phase CGM contributes a diffuse gas background that exerts additional (ram) pressure, which can counteract outflow expansion (Shin et al. 2021). While the CGM is diffuse, it is expected to follow a shallow density profile that would slow the outflow's expansion once the swept-up CGM mass becomes comparable to  $M_{\infty}$ . This occurs at a height of  $z_{\text{CGM}} \sim 5 \sigma_1 n_0^{-1/6} n_{\text{CGM},-3}^{-1/3}$  kpc, where  $n_{\text{H, CGM}} = 10^{-3} n_{\text{CGM},-3} \text{ cm}^{-3}$  is the number density of hydrogen in the CGM.

**Ejecta Mass.** For the asymptotic steady-state solution, we consider a limit where the outflow has traveled sufficiently far above the disk, yet is not old enough for its mass to be dominated by the ejecta. The timescale for the outflow to become ejecta-dominated is  $t_{\text{ED}} \sim 4\pi M_{\infty}/\dot{M}_{\text{SB}} \sim 12.6 \sigma_1^3 n_0^{-1/2} M_{\text{ej},0}^{-1} \mathcal{R}_{-3}^{-1}$  Gyr, which is considerably longer than the lifetime of the starburst driving the outflow. We therefore consider our results to be robust against this approximation.

**Thin-Shell and Sector Approximation.** While the thin-shell approximation is well-suited for radiative blastwaves or those propagating through media with positive density gradients, it becomes increasingly crude in environments with steep negative density gradients. This is because the mass, energy, and momentum distributions behind the shock broaden significantly (see e.g. Laumbach & Probstein 1969; Koo & McKee 1990). Despite the steep density gradient considered in this work, our model focuses on a radiative, momentum-driven wind, where the thin-shell approximation is expected to remain reasonably accurate. The sector approximation, on the other hand, is most reliable when the local shock surface remains relatively flat. This approximation can break down if adjacent streamlines begin to diverge significantly, e.g. due to sudden deflections. However, since observed outflows generally exhibit large opening angles,

this approximation is likely to have only a negligible impact on our findings.

**Treatment of CRs.** Our treatment of CRs involves a number of simplifications. While we do not explicitly account for CR cooling or interactions within the flow, this is well justified given the relevant timescales (see Appendix A.1). However, future studies with more detailed CR propagation modeling may yield different quantitative results, particularly if a detailed CR transport model within the halo is included. Such models could alter the distribution of halo CRs (Recchia et al. 2021), and reveal the microphysical impacts of CRs on outflows, including re-acceleration processes and interactions with complex magnetic field structures at the outflow–halo interface (see, e.g. Hopkins et al. 2023). Additionally, our study does not consider the spectral evolution of CR particles, which could influence the coupling between CRs and the outflowing wind fluid, potentially modifying their driving efficiency and altering observable CR emission signatures. Future work incorporating these effects could provide a clearer understanding of how CRs shape the development of outflows in CR-rich galaxy halos.